Sphingolipid distribution at mitochondria-associated membranes (MAMs) upon induction of apoptosis[S]

Vincent Mignard,[1],*,[†] Nolwenn Dubois,[1],*,[†] Didier Lanoé,*,[†] Marie-Pierre Joalland,*,[†] Lisa Oliver,*,[§] Claire Pecqueur,* Dominique Heymann,*,[†] François Paris,[2],*,[†] François M. Vallette,[2],*,[†] and Lisenn Lalier[2],*,[†]

CRCINA,* INSERM, Université d'Angers, Université de Nantes, Nantes, France; LaBCT,[†] ICO, Saint Herblain, France; and CHU de Nantes,[§] Nantes, France

ORCID IDs: 0000-0002-7612-1672 (C.P.); 0000-0003-0802-0519 (F.M.V.)

Abstract The levels and composition of sphingolipids and related metabolites are altered in aging and in common disorders such as diabetes and cancers, as well as in neurodegenerative, cardiovascular, and respiratory diseases. Changes in sphingolipids have been implicated as being an essential step in mitochondria-driven cell death. However, little is known about the precise sphingolipid composition and modulation in mitochondria or related organelles. Here, we used LC-MS/MS to analyze the presence of key components of the ceramide metabolic pathway in vivo and in vitro in purified ER, mitochondria-associated membranes (MAMs), and mitochondria. Specifically, we analyzed the sphingolipids in the three pathways that generate ceramide: sphinganine in the de novo ceramide pathway, SM in the breakdown pathway, and sphingosine in the salvage pathway. We observed sphingolipid profiles in mouse liver, mouse brain, and a human glioma cell line (U251). We analyzed the quantitative and qualitative changes of these sphingolipids during staurosporine-induced apoptosis in U251 cells. Ceramide (especially C16-ceramide) levels increased during early apoptosis possibly through a conversion from mitochondrial sphinganine and SM, but sphingosine and lactosyl- and glycosyl-ceramide levels were unaffected. We also found that ceramide generation is enhanced in mitochondria when SM levels are decreased in the MAM. This decrease was associated with an increase in acid sphingomyelinase activity in MAM.[JLR] We conclude that meaningful sphingolipid modifications occur in MAM, the mitochondria, and the ER during the early steps of apoptosis.—Mignard, V., N. Dubois, D. Lanoé, M-P. Joalland, L. Oliver, C. Pecqueur, D. Heymann, F. Paris, F. M. Vallette, and L. Lalier. **Sphingolipid distribution at mitochondria-associated membranes (MAMs) upon induction of apoptosis.** *J. Lipid Res.* 2020. **61:** 1025–1037.

Supplementary key words apoptosis • acid sphingomyelinase • ceramide • mitochondrial outer membrane permeability • lipid metabolism • cell signaling

Lipids are present as structural components of membranes but are also, through their interactions with proteins, instrumental in many cellular functions under both normal and pathophysiological situations (1). In addition to global composition, distribution of lipids among intracellular membranes is essential for cell growth, function, and survival, as it participates directly and indirectly in the cellular compartmentalization of major signaling pathways (1).

This is particularly true for sphingolipids, which are present in plasma and intracellular organelle membranes where they are involved in their structures as well as in signal transduction. Sphingolipids are divided into several species that include sphingosine, ceramides, and SM, which are metabolically and structurally related but exhibit different biological properties (2). In particular, the hydrophobic properties of the sphingolipids, which are determined by the high number of carbons in the fatty acid chains linked to the sphingoid backbone, impact on the biological responses. Alterations in sphingolipid metabolites are related to aging and common pathologies such as diabetes and cancers, and neurodegenerative, cardiovascular, and respiratory diseases (3). Sphingolipids are involved in the process of apoptosis either through clustering of lipid microdomains or as second messengers by binding specific proteins and regulating their phosphorylation (2).

Ceramides with various lengths in fatty acid chains are formed in different cell compartments or membranes by a variety of mechanisms, which enable specific, rapid, and

transient production following a given stimulus (4, 5). During apoptosis, sphingolipids can affect mitochondria through different mechanisms such as ceramide-formed channels, which could participate in mitochondrial outer membrane permeability (MOMP), kinase activation, and inhibition of respiration (1–6). Of note, ceramide metabolites can have opposite effects: for example, sphingosine-1-phosphate (S1P) signaling inhibits ceramide-mediated apoptosis in endothelial cells (7). Other results highlight the importance of compartment-specific lipid-mediated cell death and the many partners implicated in this process (8).

It has been shown that ceramide induces cell death specifically when generated in mitochondria (9). Recently, a direct implication of sphingolipids in MOMP has been further highlighted by a study showing the cooperation of microsomal sphingolipids (namely S1P and its metabolite hexadecenal) with pro-apoptotic members of the BCL-2 family, respectively BAK and BAX, to promote cytochrome c release (10). These data suggest that nonmitochondrial membranes are necessary to provide an appropriate sphingolipid environment for the executive phase of apoptosis. Indeed, ceramide has been shown to be present in the so-called mitochondria-associated membranes (MAMs), an elusive structure that connects the ER to mitochondria (11, 12). Primitively, MAM functions have been assigned to lipid transfer from the ER to mitochondria and to Ca^{2+} exchange between the two organelles (13). The protein composition of MAMs appears to be tissue-specific with a corpus of proteins mainly involved in mitochondrial functions (14). Recently, new roles have been attributed to MAMs, including the control of autophagy/mitophagy, mitochondrial fusion/fission, and apoptosis (13). This structure has also been implicated in the basic mechanisms of neurodegenerative diseases and diabetes (15–17). However, the precise molecular mechanisms and actors implicated in MAM function in such an essential program as apoptosis remain poorly characterized. Because many MAM functions appear to be similar to those implicating sphingolipids (18), we analyzed the composition of the main subspecies of sphingolipids and related enzymes in vivo and in vitro under resting and apoptotic conditions. MS allows analysis and quantification with reproductive accuracy of a large number of lipid species and subspecies in a very small amount of biological samples of diverse origins (cell, cell medium, tissue, blood, etc.). In this work, we used these properties to attempt to define the distribution of a large number of sphingolipids and their different subspecies between ER, MAM, and mitochondria by LC-MS/MS.

MATERIALS AND METHODS

Cell culture

The U251 cell line was grown in DMEM (4.5 g/l glucose) supplemented with 10% FCS, antibiotics (penicillin, streptomycin), and glutamine (Life Technologies, Carlsbad, CA) in 5% CO_2 at 37°C. Apoptosis was induced in cultures at 70% confluency with 0.5 μg/ml staurosporine (STS; Santa Cruz Biotechnology, Heidelberg, Germany).

Subcellular fractionation

Livers from C57BL6 mice (about 10 g) or U251 cells from 40 petri dishes (representing about 16×10^7 cells) were homogenized and subcellular fractionation prepared by differential centrifugation as previously described (19). Briefly, after homogenization, unbroken cells and nuclei were removed, and then an intermediate pellet was isolated from a fraction later centrifuged for ER and cytosol isolation and finally separated by ultracentrifugation (20,000 g for 30 min and then 100,000 g for 1 h). The crude mitochondrial fraction (MF) was obtained by centrifugation of the previous resuspended pellet at 10,000 g for 10 min. Crude MF was then layered on top of 30% Percoll medium and centrifuged at 95,000 g for 30 min. After this centrifugation, a dense band of pure mitochondria (PM) was observed at the bottom of the tube and a diffused white band of MAM at the top of the tube. These fractions were collected with a Pasteur pipette, diluted, and then pelleted respectively at 6,300 g for 10 min and 100,000 g for 1 h. The different fractions were diluted in different volumes as described in supplemental Fig. S1.

Immunoblot analysis

For Western blot analysis, 10 μg total protein (cells) or 30 μg (liver) from each fraction (supplemental Fig. S1) were loaded onto 8% or 12% SDS-PAGE and transferred onto Immobillion-P transfer membrane (Millipore, Darmstadt, Germany) for immunoblotting. The primary antibodies used were anti-FACL-4 (ACSL-4) (sc-365230; Santa Cruz Biotechnology), anti-calreticulin (CR) (c1036; US Biological, Salem, MA), anti-VDAC (V2139; Sigma-Aldrich, St Louis, MO), anti-cytochrome c (7H82C12; R&D Systems, Minneapolis, MN), anti-TOM20 (sc-11415; Santa Cruz Biotechnology), anti-RTN3 (sc-374599; Santa Cruz Biotechnology), and anti-LAMP2 (PA5-85327; Thermo Fisher Scientific).

Microscopy

Transmission electron microscopy was done on cells fixed with 4% glutaraldehyde in PBS (pH 7.4) followed by a postfixation with 2% OsO_4. After dehydration in a graded series of ethanol, adherent cells were embedded in epoxy resin, and thin sections (60 to 70 nm) were cut on a Reichert Ultracut E microtome and stained with uranyl acetate and lead citrate for observation at 80 KV under a JEM-1010 transmission electron microscope (JEOL).

For microscopic analyses, cells were grown on gelatin-coated coverslips. The cells were incubated with MitoTracker Red (Life Technologies) for 30 min at 37°C, washed two times with PBS, and then fixed in 4% paraformaldehyde for 30 min. The cells were washed with PBS and then mounted with Prolong antifade (Life Technologies) polymerizing solution and observed under a microscope with a 63× objective (Zeiss with apotome).

FACS analysis

Cells treated or not treated with STS were harvested after 2, 4, 6, or 8 h, permeabilized in PBS/0.002% digitonin, and fixed for 15 min with 2% paraformaldehyde. Cytosolic cytochrome c is lost during mild digitonin-induced membrane permeabilization, apoptotic cells thus appear negative for cytochrome c staining. Staining for cytochrome c (Clone 6H2.B4; BD Biosciences, San Jose, CA) and active Bax (Clone 6A7; BD Biosciences) was performed overnight at 4°C. The percent of positive cells was determined compared with isotype. For cell viability assessment, cells were harvested after STS treatment and the number of dead PI positive cells was determined after 5 min incubation with propidium iodide (Sigma).

Lipid extraction

The internal standard mixture composed of C17 ceramide, C17 SM, C17 sphingosine-1-phosphate, C12 ceramide-1-phosphate, C17 sphinganine, C12 lactosyl-ceramide, and C12 glucosyl-ceramide was added to each biological sample. Lipid extraction was carried out in two steps. First, 1.5 ml of hexane/propan-2-ol (60:40, v/v) containing 0.6% formic acid were added, samples were centrifuged at 1,000 g for 5 min (4°C), and the upper phase was removed into a glass tube. Then, 1.5 ml of methanol containing 0.6% formic acid were added to the lower phase. After centrifugation at 7,000 g for 5 min (4°C), the two upper phases were combined and dried under nitrogen at room temperature. The total lipid extract was suspended in 150 μl of hexane/propan-2-ol (60:40 v/v) (0.6% formic acid).

Lipid purification

Targeted lipid purification was carried out using NH_2 SPE cartridges (100 mg). Total extract was deposited on cartridges preconditioned with 2 ml of hexane. Different classes of lipids were separated following the method described in (20). The four recovered fractions (F2, F4, F5, and F6) were dried down under nitrogen and removed in optimized volume of UPLC eluent A.

UPLC-ESI-MS/MS analysis

The sphingolipids were quantified by LC-ESI-MS/MS. The purified sphingolipids were analyzed on an Acquity H-Class UPLC system (Waters Corporation, Milford, MA) combined with a Waters Xevo TQD triple quadrupole mass spectrometer. All analyses were performed using ESI in the positive ion mode (ESI+) with multiple reaction monitoring. All sphingolipid classes were analyzed on a Waters C18 BEH column (2.1 × 50 mm) with 1.8 μm particle size equipped with a 0.5 μM prefilter. The column heater was set at 43°C for all compounds except ceramide-1-phosphate and sphingosine-1-phosphate where column temperature was set at 60°C. The autosampler temperature was maintained at 10°C. The mobile phases consisted of methanol (eluent A) or water (eluent B) containing 1% formic acid and 5 mM of ammonium formate. Purified sphingolipid fractions (sample and calibration) were eluted according to the elution step program.

Measurement and data analysis were collected by Mass Lynx software version 4.1 (Waters, Manchester, UK). Integration and quantification were performed using the TargetLinks™ software (Waters).

Sphingomyelinase activity

Acid sphingomyelinase (ASMase) and neutral sphingomyelinase (NSMase) enzymatic activities were determined using the fluorescent substrate BODIPY-FL-C12-SM (Invitrogen-Life Technologies; D-7711).

ASMase reaction (21) was initiated by the addition of 1 μg protein sample in a volume of 100 μl containing 73 pmol substrate in 12.5 mM sucrose buffer (pH 5.0) with 1% Triton X-100 and 0.1 mM of $ZnCl_2$ or 5 mM of EDTA activation buffer. EDTA and $ZnCl_2$ buffers were used respectively for lysosomal ASMase (L-ASMase) and total ASMase activity quantification.

NSMase activity was magnesium dependent (22). The reaction was initiated by 1 μg of protein sample in a volume of 100 μl containing 10 pmol of substrate in 200 mM of HEPES buffer (pH 7.4) with 20 mM of $MgCl_2$.

The reaction was processed at 37°C over 24 h and stopped by adding chloroform:methanol (1:1, v/v). Samples were centrifuged at 1,000 g for 5 min. The organic phase was harvested, evaporated under N_2, and resuspended in chloroform/methanol (2:1, v/v).

Five microliters were spotted on silica gel 60 thin-layer chromatography plates (Merck-Millipore; 105626). Ceramide and uncleaved SM were separated using a mixture of chloroform:methanol (95:5, v/v) as a solvent and were quantified on a ChemiDoc MP imaging system (Bio-Rad) with the ImageLab software (Bio-Rad). Enzymatic activity is presented as the hydrolysis rate of SM (picomoles) per time (hours) and per protein concentration (micrograms).

Statistical analysis and animal studies

Two-way ANOVA and, as posttest, Tukey's multiple comparison test were used in this study. Research involving animals were performed in agreement with the French National Ethics Committee. Investigations with animals were approved by the local institutional review committee of the animal house facilities.

RESULTS

ER, MAM, and mitochondria sphingolipid composition in mouse liver

We first analyzed the mitochondrial and ER proteins present in the different submembrane fractions from mouse liver by immunoblots (see the Materials and Methods). As illustrated in **Fig. 1A**, we found a repartition of these different proteins from ER to MAM to MF similar to that described in previous studies: CR (23) and the long-chain fatty acid-CoA ligase 4 (FACL-4) (24) were found in ER and MAM, while VDAC1 and cytochrome c were predominantly found in mitochondria. Similar but not identical results were found in mouse brain (supplemental Fig. S2).

Next, we analyzed and quantified the sphingolipid content and, in particular, precursors and metabolites of ceramides in the different liver fractions by LC-ESI-MS/MS. Ceramides and SM were present mostly in MAM and the ER (Fig. 1B). On the other hand, sphinganine was essentially present in MAM and PM fractions, while sphingosine was found mostly in PM (Fig. 1C). Statistical data for lipid measurements are shown in supplemental Fig. S3.

Glycosylated forms of ceramides are biologically active and versatile derivatives of ceramides. These glucosyl- and lactosyl-ceramides are thought be synthesized in the late ER compartments. although there is some evidence that they are present in MAM (11). We confirmed the latter observation and found that, in mouse liver, glucosyl-ceramide is essentially present in MAM, while lactosyl-ceramide is located both in PM and MAM (Fig. 1D).

Analysis by the chain lengths of the sphingolipids shows some differences between the different fractions: MAM and PM fractions were enriched in C18 compared with ER, while ER and PM fractions were enriched in C24 and C24:1 compared with MAM (**Table 1**). However, major and minor chain lengths in the different fractions appear to be roughly constant and no chain length is specific from any organelle (except from C18 ceramide, which is the only ceramide found in cytosol) (Table 1).

Our data support previous observations on the presence of sphingolipids in MAM. However, sphingolipids present
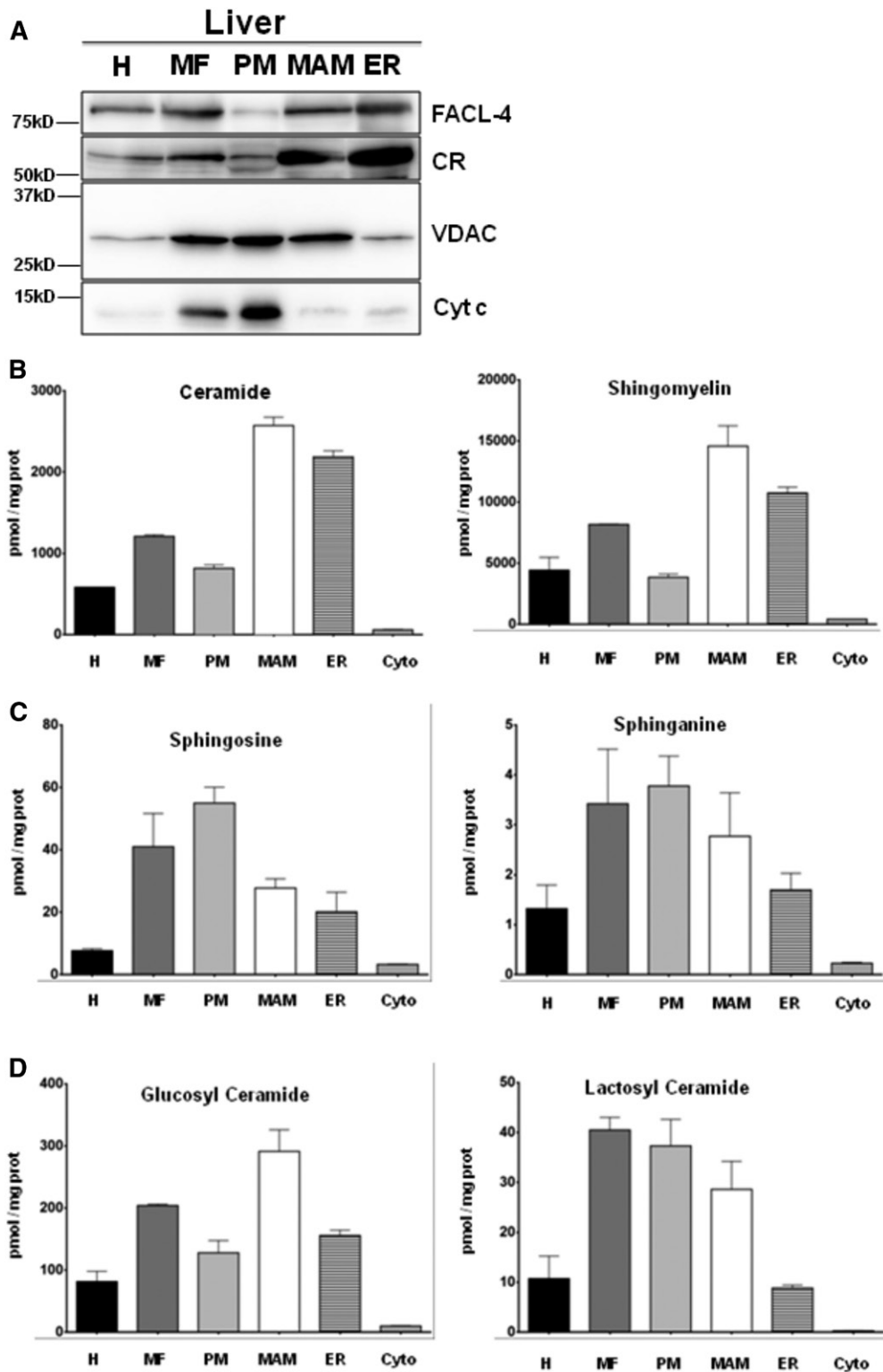
Fig. 1. Subcellular fractionation performed on mouse livers. A: After fractionation, 30 μg of total protein from each fraction are loaded on 12% SDS-PAGE to analyze the distribution of mitochondrial [VDAC, cytochrome c (Cyt c)] and ER (FACL-4, CR) markers. B–D: Lipid extraction and purification are done from 50 μl of each fraction (H, homogenate; Cyto, cytosol). The sphingolipid compositions of the fractions are then analyzed by UPLC-MS. The results are expressed in picomoles of lipid per milligram of proteins. For ceramide, SM, glucosyl-ceramide, and lactosyl-ceramide, the results represent the cumulative amount of all chain lengths (mean ± SEM).

TABLE 1. Subcellular fractionation performed from mouse livers

	H		MF		PM		MAM		ER		Cyto	
	Mean	SEM	Mean	SEM	Mean	SEM	Mean	SEM	Mean	SEM	Mean	SEM
Ceramide												
C14:0	4.87	1.61	7.11	1.25	9.10	3.96	4.72	1.49	10.47	2.07	0.51	0.37
C16:1	1.25	0.58	1.98	0.28	3.72	1.10	2.57	0.60	1.43	0.41	0.85	0.42
C16	38.76	12.63	78.41	10.11	112.00	34.92	58.63	17.82	97.24	13.90	3.51	0.52
C18:1	0.93	0.31	2.03	0.27	3.84	1.07	0.29	0.29	1.13	0.29	0.19	0.19
C18	32.37	7.77	137.45	28.70	144.17	22.86	204.34	56.83	54.82	8.11	152.20	34.72
C20:1	0.00	0.00	0.00	0.00	0.00	0.00	0.00	0.00	0.00	0.00	0.00	0.00
C20	1.64	0.60	4.09	0.64	8.86	4.07	2.81	0.54	6.05	1.34	0.25	0.25
C22:1	1.09	0.38	2.27	0.58	4.08	1.88	1.35	0.29	4.24	0.49	0.00	0.00
C22	7.59	2.52	18.14	2.10	35.72	11.37	12.84	4.17	25.24	4.06	1.30	0.05
C24:1	123.55	41.27	258.84	29.87	445.91	131.01	173.11	48.49	358.68	36.25	11.39	2.48
C24	40.53	14.50	84.53	7.12	131.50	35.35	57.68	13.29	120.36	13.37	6.17	1.17
SM												
C14:0	317.93	68.99	1,464.30	106.82	593.72	131.79	1608.66	64.32	993.28	135.61	21.61	10.82
C16:1	376.22	81.26	1,708.56	97.20	672.38	123.04	1,852.92	28.60	1,135.45	158.04	36.65	3.90
C16	4,653.71	880.03	22,298.32	2,219.49	9,495.85	1,969.88	24,336.04	714.99	13,682.74	1,602.26	906.61	389.91
C18:1	112.37	25.73	470.80	45.54	192.90	24.54	513.99	23.53	307.04	24.20	6.50	3.58
C18	422.00	79.76	2,019.36	88.37	981.44	183.30	2,030.76	31.16	1,152.21	137.07	119.18	73.24
C20:1	18.76	5.59	74.43	10.07	35.55	3.01	65.03	8.90	51.85	8.20	0.00	0.00
C20	81.09	19.07	406.08	35.36	157.10	22.46	382.61	39.81	223.89	32.96	57.25	54.12
C22:1	116.03	18.77	529.34	34.78	224.42	28.59	543.24	31.37	315.91	46.55	19.85	14.53
C22	204.01	40.39	1,108.36	132.84	475.91	96.14	1,014.94	141.00	551.23	78.40	22.84	13.53
C24:1	1,656.56	257.77	8,205.66	1,135.30	3,683.24	932.79	8,478.13	442.03	4,878.83	917.29	385.63	170.81
C24	371.86	53.23	2,049.34	333.96	898.11	235.67	1,839.27	232.73	1,096.05	221.38	368.50	323.24
Sphingosine												
C18:1	21.66	4.01	113.35	18.81	213.25	27.40	128.50	71.59	23.56	5.10	61.79	18.04
Sphinganine												
C18	2.31	0.56	12.18	1.86	34.56	1.96	5.13	2.24	2.32	0.35	1.53	0.48
Glucosyl-ceramide												
C14:0	0.00	0.00	0.01	0.01	0.00	0.00	0.01	0.01	0.01	0.01	0.00	0.00
C16:1	0.51	0.13	2.86	0.27	1.73	0.31	1.99	0.03	1.76	0.04	0.00	0.00
C16	50.62	11.05	252.43	3.77	199.79	18.40	197.40	12.31	127.85	9.44	4.15	0.40
C18:1	0.14	0.08	0.64	0.33	0.72	0.36	0.31	0.31	0.25	0.12	0.00	0.00
C18	3.98	1.03	21.57	1.23	17.76	2.21	18.60	2.38	9.04	0.81	0.12	0.12
C20:1	0.07	0.07	0.00	0.00	0.30	0.30	0.07	0.07	0.11	0.09	0.00	0.00
C20	1.12	0.18	6.38	0.26	5.73	0.50	5.74	0.39	2.14	0.07	0.04	0.04
C22:1	5.86	1.29	32.69	2.48	28.52	1.77	24.07	2.45	12.70	1.29	0.17	0.17
C22	0.25	0.17	1.28	0.66	1.37	0.69	0.89	0.49	0.45	0.23	0.01	0.01
C24:1	44.09	8.69	255.23	10.99	242.01	13.46	166.90	16.72	99.79	8.43	3.53	0.53
C24	30.63	7.12	154.09	11.89	126.75	4.81	111.96	10.42	84.62	7.46	2.02	0.38
Lactosyl-ceramide												
C14:0	1.13	0.55	4.83	1.51	1.72	0.51	4.31	0.90	3.51	0.51	0.00	0.00
C16:1	0.06	0.06	0.28	0.28	0.07	0.07	0.50	0.29	0.25	0.12	0.00	0.00
C16	55.57	25.53	240.49	63.68	101.18	22.27	263.90	54.47	176.60	33.99	3.99	1.49
C18:1	0.64	0.35	1.87	0.64	0.92	0.14	1.19	0.75	1.17	0.22	0.00	0.00
C18	6.21	3.04	28.88	9.89	12.97	3.15	36.23	10.41	16.44	3.91	0.54	0.54
C20:1	0.01	0.01	0.10	0.10	0.01	0.01	0.07	0.07	0.04	0.04	0.00	0.00
C20	0.31	0.14	1.61	0.42	0.94	0.15	2.68	0.38	0.87	0.10	0.00	0.00
C22:1	0.31	0.12	1.34	0.49	0.35	0.35	1.47	0.74	0.66	0.20	0.00	0.00
C22	3.08	1.17	17.18	3.59	8.34	1.95	25.20	4.28	8.62	1.52	0.24	0.24
C24:1	34.72	11.85	203.00	54.79	115.16	30.89	320.84	78.76	103.84	21.41	5.83	2.08
C24	19.11	7.16	89.54	14.31	42.22	6.60	118.84	16.18	57.39	5.01	1.80	0.55

Lipid extraction and purification were performed on 50 µl of each fraction. The sphingolipid composition of the fractions was then analyzed by UPLC-MS. The results are expressed in picomoles of lipids per milligram of proteins for each chain length of ceramide and SM (mean ± SEM). Cyto, cytosol; H, homogenate.

in MAM are quantitatively and qualitatively different from those found in ER and mitochondria.

Sphingolipid composition of ER, MAM, and U251 in U251 cells: effect of the induction of apoptosis

Sphingolipids have been implicated in apoptosis, but little is known about their intracellular distribution between ER, MAM, and mitochondria during the induction of this cell death program (8). Induction of apoptosis in liver is a multimodal and complex phenomenon that involves different processes. In order to obtain a more homogeneous population, we investigated the sphingolipid composition in resting and apoptotic human glioma U251 cells. This cell line has been extensively studied as a model for apoptosis (25). As illustrated in **Fig. 2A**, transmission electron microscopy studies reveal that U251 cells exhibited ER/mitochondria contacts that resemble classical MAM morphology. Resting U251 cells were subjected to subcellular fractionation as described in the Materials and Methods (19). We first analyzed by immunoblots using various markers of mitochondria and ER proteins specific for the different fractions. As illustrated in Fig. 2B, we found a classical
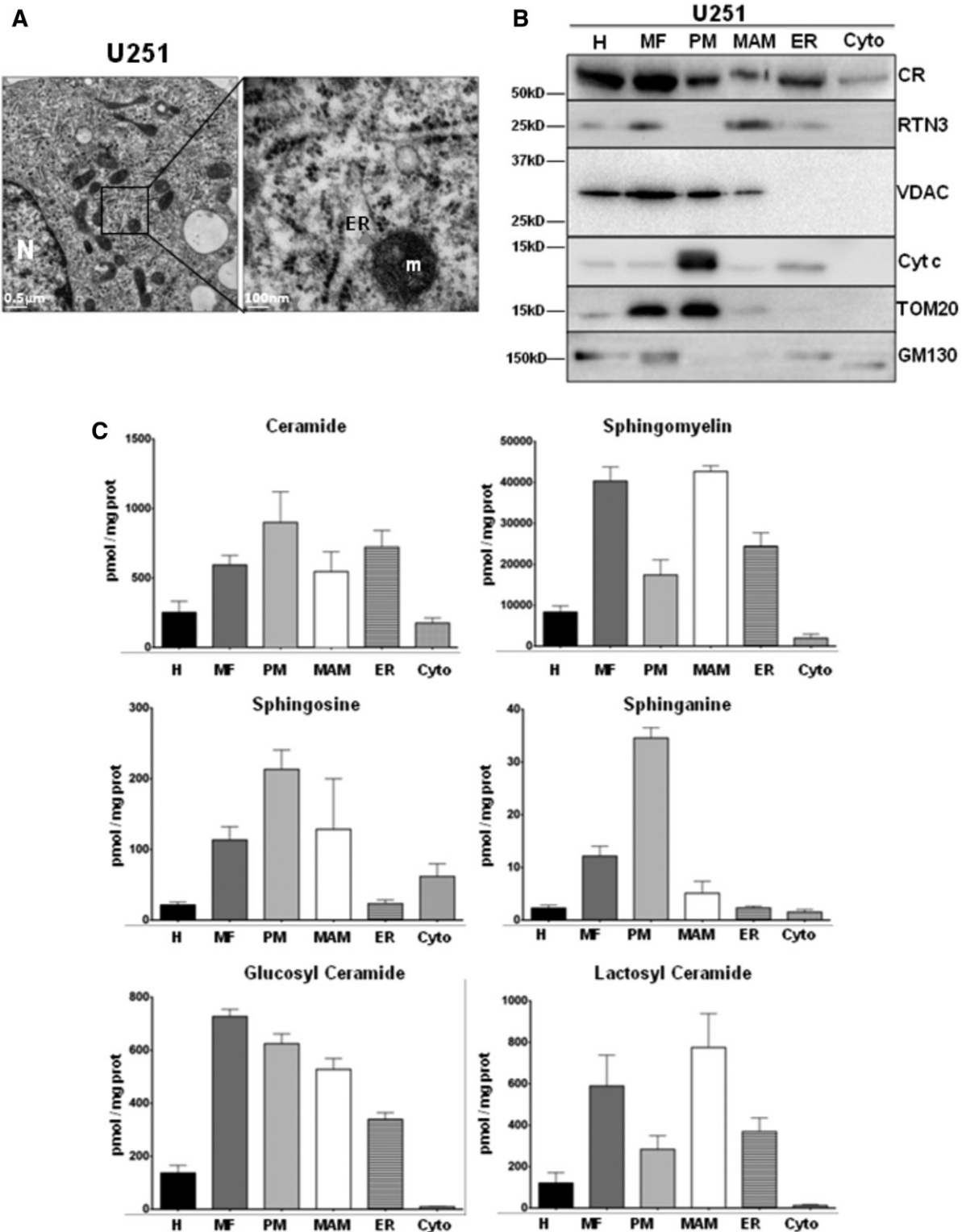
Fig. 2. Subcellular fractionation performed on U251 cells. A: Observation of U251 cells by transmission electron microscopy. Subcellular structures like nucleus (N), mitochondria (m), and ER tubules with ribosomes are observable here (left panel, the bar represents 0.5 μm). At higher magnification, close appositions between mitochondria and ER tubule are visible (red arrowhead). In this image, the ER tubule undergoes a deformation at the contact region with a mitochondrion (right panel, the bar represents 100 nm). B: After fractionation, 10 μg total protein of each fraction are loaded on 12% SDS-PAGE to analyze the distribution of mitochondrial [VDAC, cytochrome c (Cyt c), TOM20], ER (CR, RTN3), and Golgi (GM130) markers. C: Lipid extraction and purification are done from 50 μl from each fraction. The sphingolipid compositions of the fractions are then analyzed by UPLC-MS. The results are expressed in picomoles of lipid per milligram of proteins. For ceramide, SM, glucosyl-ceramide, and lactosyl-ceramide, the results represent the cumulative amount of all chain lengths (mean ± SEM).

repartition of these different proteins from ER to MAM and MF: CR and RTN3 (14) were found in ER and MAM, while VDAC, TOM20, and cytochrome c were predominantly found in mitochondria; GM130 was slightly detected in the ER fraction, suggesting a mild contamination with Golgi membranes. We examined the sphingolipid composition of the different fractions and found that, at variance with mouse liver, ceramide and SM were partitioned between PM, MAM, and ER, and sphingosines were localized in MAM and PM while sphinganine was essentially mitochondrial (Fig. 2C). Of note, the ratio of glycosylated ceramides in the different subcellular compartments was inverted compared with mouse liver (Fig. 2C).

Next, we monitored the kinetics of the induction of apoptosis in STS-treated cells by analyzing the disruption of the mitochondrial network. As shown in **Fig. 3A**, the mitochondrial network in STS-treated cells was maintained at 2 h but started to be disrupted at 4 h. The main cellular events leading to apoptotic cell death in STS-treated U251 cells can be defined by first a change in the conformation of the pro-apoptotic protein Bax [monitored by the monoclonal 6A7 (26)] and the release of cytochrome c (released cytochrome c is lost during washing steps in the permeabilized cells; apoptotic cells are thus cytochrome c negative) as a demonstration of the apoptotic MOMP (Fig. 3B, left and middle graphs). The final step of cell death can be quantified by the induction of nonselective plasma membrane permeability visualized by propidium iodide staining (Fig. 3B, right graph). Based on the different results, we define a chronology of apoptotic cell death in U251 cells

with early apoptotic events taking place before 2 h of STS treatment. Subcellular fractionation indicates that during the early mitochondrial-dependent apoptotic events, there are no major changes in protein distribution between ER/MAM/PM (Fig. 3C).

Next, we examined the sphingolipid contents 2 and 4 h after the induction of apoptosis. No change in the total cellular concentrations of glucosyl- and lactosyl-ceramides is observed under these conditions until 4 h (**Fig. 4A**). However, a significant decrease in sphingosine and SM concentrations is observed in U251 cells after 2 h of STS treatment, while total cellular sphinganine content decreases only at 4 h. An increase in ceramide is observed at 4 h (Fig. 4A), which corresponds to a significant rise in C16 ceramide (Fig. 4B), a form shown to be associated with apoptosis (27). Thus, a modification in the expression of sphingolipids, in particular ceramide C16, closely accompanies the first steps of mitochondrial apoptosis, as previously shown for UV-induced apoptosis (28).

Subcellular distribution of sphingolipids and related enzymes in apoptotic U251 cells

To further substantiate this assertion, we analyzed the distribution of sphingolipids in the different organelles of U251 cells at 2 and 4 h after the induction of apoptosis by STS (i.e., maximum Bax activation analyzed by exposure of the 6A7 epitope and the onset of cytochrome c release from mitochondria, see Fig. 3). We observe an important increase in ceramide content in PM 4 h after STS treatment (**Fig. 5A**). In contrast, the content in SM is specifically
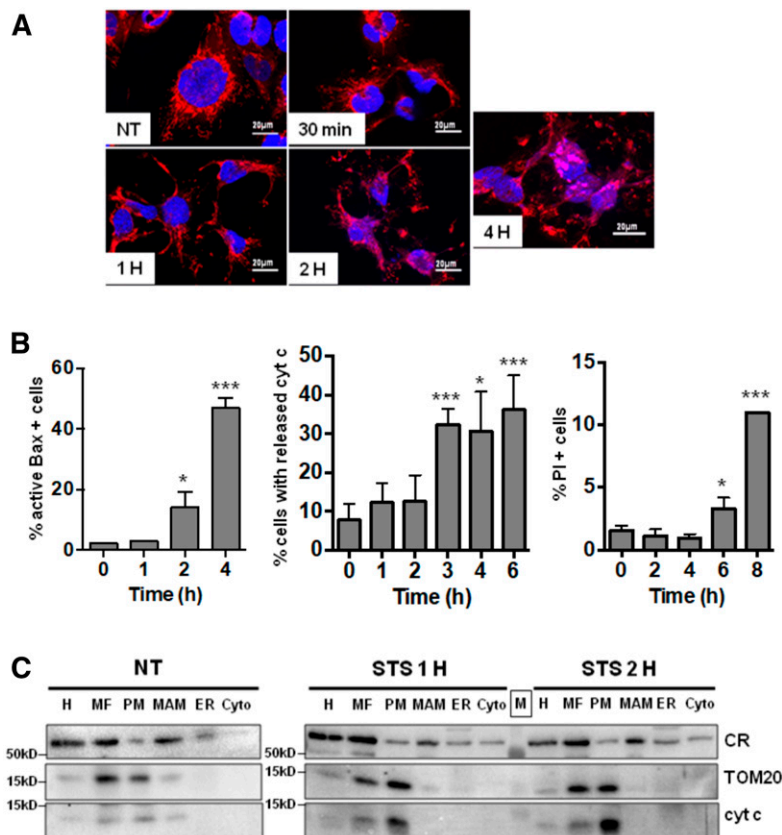

Fig. 3. Induction of apoptosis by STS-treatment in U251 cells. A: Impact of STS-induced apoptosis on mitochondrial network. Polarized mitochondria are stained by Mitotracker (red) and nucleus with Dapi (blue) (scale bar represents 20 µm). B: Cells were treated by STS and stained for 6A7 active Bax (left) or cytochrome c (cyt c) (middle) as described in the Materials and Methods, or unfixed cells were stained with propidium iodide (PI) (right) and analyzed by flow cytometry (*$P < 0.05$, ***$P < 0.0001$ vs. T0). C: Impact of STS-induced apoptosis on the subcellular distribution of the fraction markers (CR, TOM20, and cytochrome c).
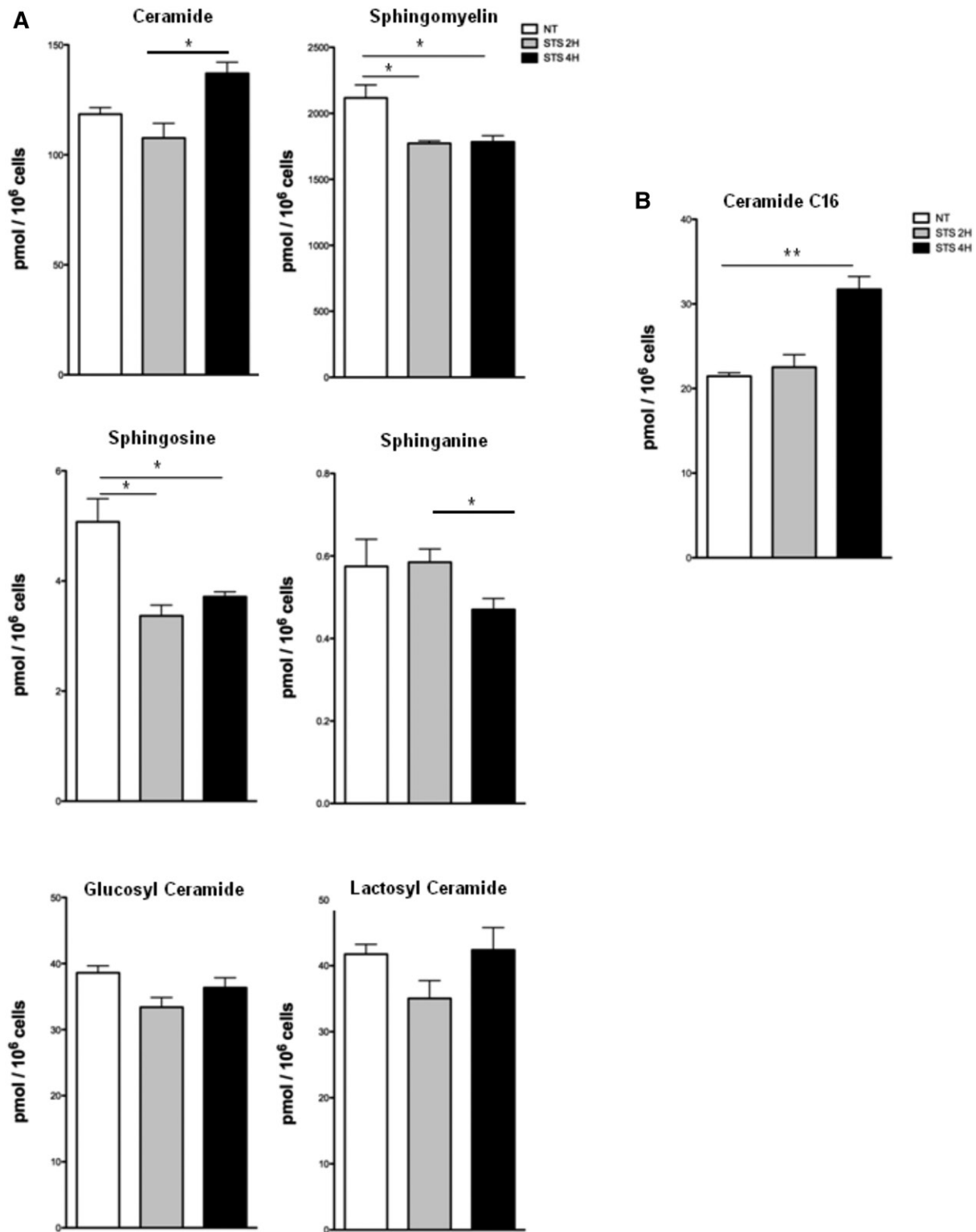
Fig. 4. Impact of apoptosis on the total cellular sphingolipid content in U251 cells. After STS treatment, lipid extraction and purification are performed from cell pellets. Sphingolipid levels are then measured by UPLC-MS. A: Cumulative amounts of all chain lengths are expressed in picomoles per 10^6 cells. B: Levels of specific C16 ceramide (picomoles per 10^6 cells) (mean ± SEM; *$P < 0.05$, **$P < 0.01$ vs. nontreated cells).

decreased in MAM (Fig. 5B). The sphingosine contents are not affected by STS treatment (Fig. 5C). Quite surprisingly, we observe a similar increase in sphinganine in mitochondria (Fig. 5D), although the global cellular concentration is decreased (Fig. 4A). On the other hand, no change in the distribution of sphingosine and glucosyl- and lactosyl-ceramides is observed (Fig. 5 E, F). Our results show that the distribution of sphingolipids in the MAM and mitochondria is regulated differently from total cellular contents.
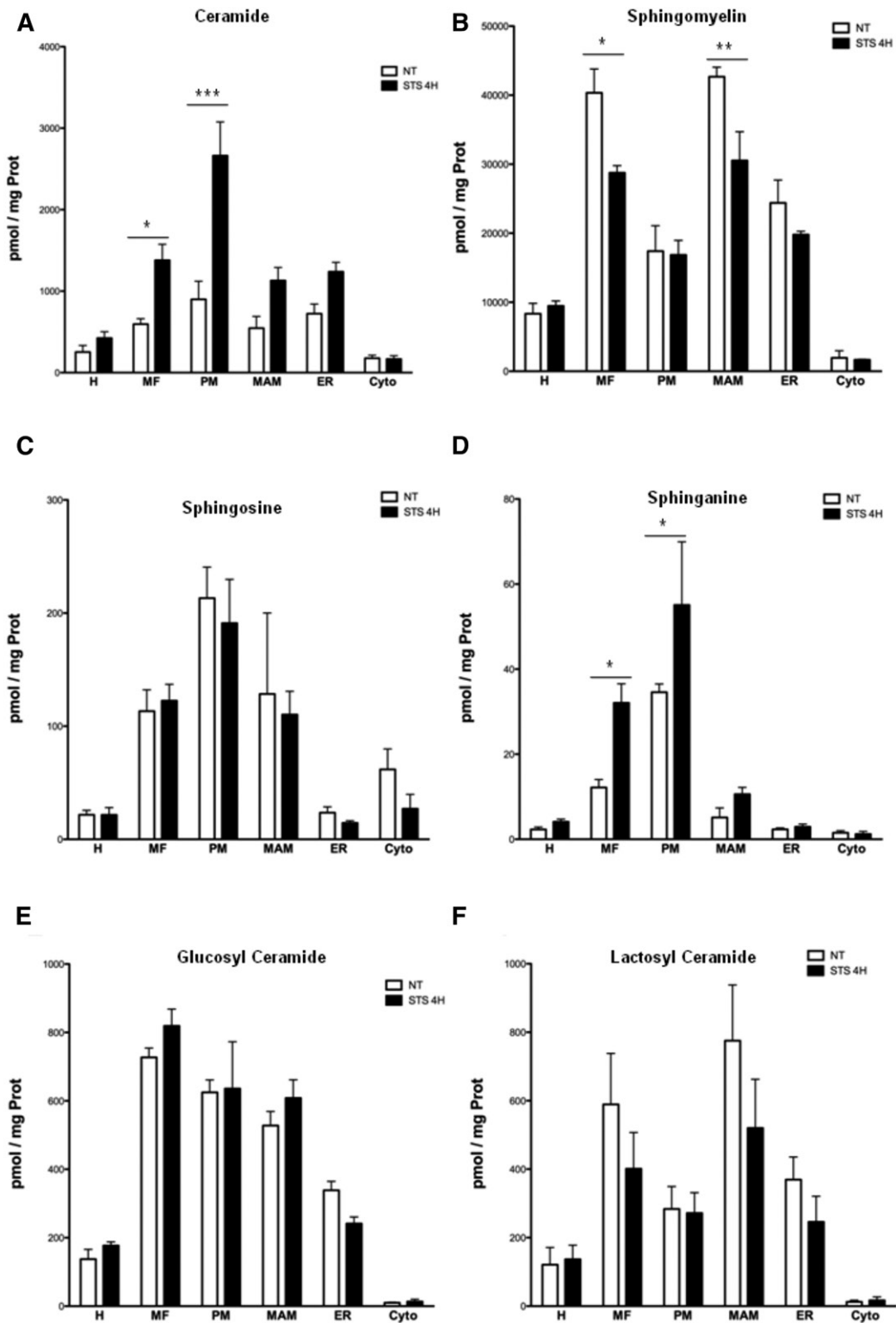
Fig. 5. Impact of apoptosis on the subcellular distribution of sphingolipids in U251 cells. Subcellular fractionation is performed from STS-treated cells. Lipid extraction and purification are done on 50 µl from each fraction. Sphingolipid levels are then analyzed by UPLC-MS and compared with control (nontreated cells). Impact of STS-induced apoptosis on subcellular levels of ceramide (total chain length) (A), SM (total chain length) (B), sphingosine (C), sphinganine (D), glucosyl-ceramide (E), and lactosyl-ceramide (F). Results are expressed in picomoles of lipid per milligram of proteins (mean ± SEM; *$P < 0.05$, **$P < 0.01$, ***$P < 0.0001$ vs. nontreated cells).

Because of the putative importance of the modulation of SM and ceramide in MAM/PM during apoptosis, we analyzed the distribution of ASMase activity [both L-ASMase and secreted ASMase (S-ASMase)] in the different organelles in U251 cells 4 h after the induction of apoptosis by STS. We observe a repeated increase in ASMase activity in MAM but not in PM (**Fig. 6A–C**, supplemental Fig. S4A). The increase in ASMase activity is statistically significant in each individual experiment but not significant when all results are compiled (supplemental Fig. S4A) due to inter-experiment variability. ASMase activity is separated into L-ASMase and S-ASMase; both L- and S-ASMase activities are increased during the early induction of apoptosis in the MAM fraction (Fig. 6B, C). As for total ASMase activity, the increase in L- and S-ASMase activity in the MAM fraction is statistically significant in each experiment but not when all data are analyzed due to important inter-experiment variation (supplemental Fig. S4A). Of note, NSMase activity is not affected during the time of treatment, in any compartment (Fig. 6D and supplemental Fig. S4A). Given the suggested association of lysosomes to the mitochondrial membranes in mitochondrial fusion sites (29), we next questioned the presence of lysosomal membranes associated to mitochondria and MAM. However, while the presence of the lysosomal protein LAMP2 is detected in all the subcellular fractions isolated (Fig. 6E), the ASMase activity is not altered in the MF and PM fraction. Of note, the microscopic observation of U251 MF reveals the regular proximity between mitochondria, ER, and lysosomes (supplemental Fig. S4B). The amount of lysosomes copurified with the MF is not increased by STS (Fig. 6F, supplemental Fig. S4C), suggesting that the increase in ASMase activity measured in MAM is not due to the recruitment of lysosomes. Of note, confocal imaging reveals that ASMase is sometimes found in the proximity to mitochondria (supplemental Fig. S5), even if no significant increase in the colocalization between ASMase and the mitochondrial marker TOM20 is observed in apoptotic cells.

DISCUSSION

Apoptosis can be initiated in many different ways, but it is generally admitted that most signals are converted into a common mechanism at the mitochondrial level, which in turn triggers the execution phase of the cell death program. Sphingolipids play a major role in the regulation of cell death and trigger different types of apoptosis depending on its intracellular localization from plasma membrane to mitochondrial outer membrane. Several studies have underlined the importance of lipids in the BCL-2 family functions (8, 10, 30, 31). Elusive structures called MAMs play a major role in the coupling between ER apoptotic signals and mitochondria mainly by supporting the ER-mitochondria transport and synthesis of lipids and calcium exchange between these two organelles (18, 32). Compartmentalization of sphingolipid-metabolizing enzymes into different subcellular locations has been extensively described (1). De novo ceramide synthesis takes place in the ER where serine and palmitoyl-

CoA are condensed into sphinganine (2). Ceramide is synthesized from sphinganine by ceramide synthases located at various membranes (ER, nuclear membrane, mitochondria, MAM) (33). Sphingosine can be recycled via the salvage pathway to regenerate ceramide. Ceramide generation can also occur via SM hydrolysis through the activity of sphingomyelinase. Based on the specific intracellular localization of sphingolipid enzymes and their products, sphingolipid functions have been largely restricted to the site of generation but may also be involved in specific functions in other subcellular compartments. For instance, little is known about the MAM-specific roles and distribution, if any, in sphingolipid metabolism. In this work, we used LC-MS/MS to define the distribution of a large number of sphingolipids and their different subspecies between ER, MAM, and mitochondria in human glioma U251 cells at the basal level and during the apoptotic process. We specifically analyzed the sphingolipids specific to the three pathways capable of generating ceramide: sphinganine for the de novo pathway, SM for the breakdown pathway, and sphingosine for the salvage pathway (2). The addition of sugar to ceramide to form complex sphingolipids was analyzed by measuring lactosyl- and glucosyl-ceramides. No significant difference was measured in the composition of the different species regarding the chain lengths during apoptosis induction. The glycosylated forms of ceramide were not altered during STS treatment (Figs. 4A; 5E, F) either at the cellular level or in the fractions. At the cellular level, ceramide (especially C16 ceramide) increased after 4 h concomitant to a decrease in sphinganine (Fig. 4A, B). These events were preceded by a decrease in the cell SM and sphingosine levels (Fig. 4A). These results suggest that the increase in ceramide induced by apoptosis induction entails several processes: first, SM hydrolysis and activation of the salvage pathway (sphingosine recycling), and then de novo synthesis of ceramide from sphinganine by ceramide synthases. At the organelle level (Fig. 5), the ceramide increase is mainly measured in mitochondria, which is consistent with the apoptotic function of ceramide described in the literature (9). We measured no concurrent SM decrease in mitochondria; however, we measured it in MAM (Fig. 5B), suggesting that SM hydrolysis occurs in MAM rather than in mitochondria, followed by ceramide transfer to mitochondria. This is consistent with the sphingomyelinase activity increase we measured in MAM but not in mitochondria (Fig. 6A–D, supplemental Fig. S4A). With reference to de novo synthesis, Fig. 5D shows that sphinganine concentration is mostly raised in mitochondria. Serine palmitoyltransferase is known as an ER-located enzyme (33). Sphinganine might thus be produced in the ER and transit to the mitochondria through the MAM to then be modified by mitochondrial ceramide synthases. Sphingosine decrease measured in total cells (Fig. 4A) is not recovered at the organelle level (Fig. 5C). This suggests that the recycling of sphingosine to ceramide happens in a compartment that we did not purify in our isolation protocol. Of note, our protocol is not intended for the purification of plasma membrane, nucleus, or late endosomes/lysosomes. Sphingosine-to-ceramide conversion is reported in the lysosomal fraction, which could account for the results we observe.
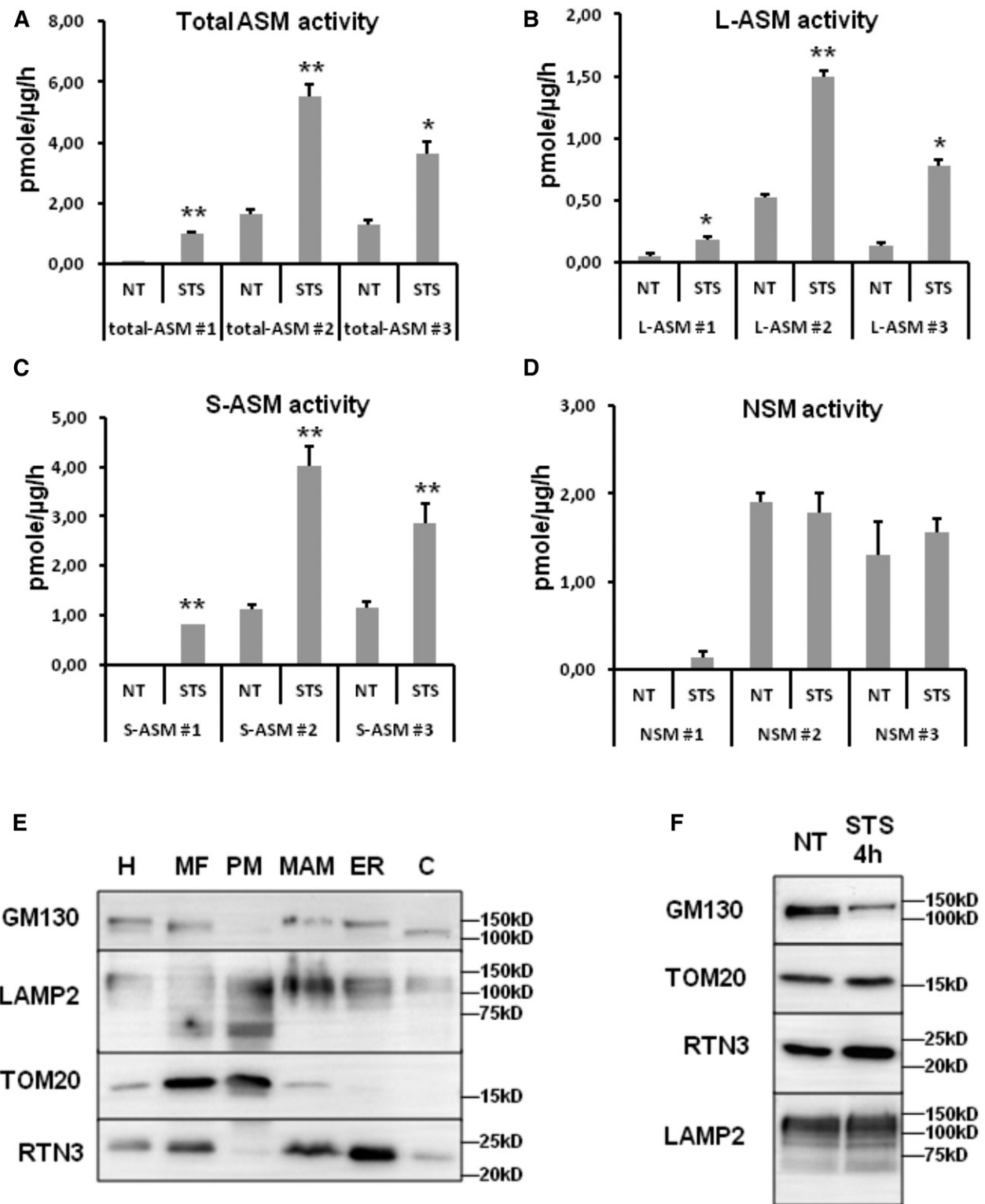
Fig. 6. Activation of ASMase subforms in the MAM fraction in the U251 cell line. Subcellular fractionation is performed from STS-treated cells. ASMase activity present in 50 μl was measured in the MAM fraction. The graphs show the results from three independent experiments. The impact of STS-induced apoptosis on total ASMase (A), L-ASMase (B), S-ASMase (C), and NSMase (D) in the MAM fraction. Results are expressed in picomoles per microgram of proteins per hour (mean ± SEM; *$P < 0.05$, **$P < 0.01$ vs. nontreated cells). E: Western blot analysis of the fractions obtained in U251 cells for the copurification of Golgi (GM130) and lysosomes (LAMP2). The blots are representative of three independent experiments. F: Western blot analysis of U251 MFs during STS treatment. The blots are representative of three independent experiments.

Thus, a quantitative and qualitative analysis of sphingolipids in the different subcellular compartments showed a different composition in the different organelles. We measured a specific activation of ASMase (L- and S- forms) in MAM during apoptosis, which could explain the decrease of SM in MAM and the concomitant increase of ceramide measured in mitochondria (Fig. 5A). ASMase activity was not typically described in MAM. We observed the copurification of lysosomes with MAM and also with other subcellular fractions (Fig. 6E). Of note, lysosome-mitochondria contacts were observed at mitochondrial fission sites (29), as were ER-mitochondria contacts. It is conceivable that tripartite ER-mitochondria-lysosomes contacts exist in cells, underlying the measurement of ASMase activity in some but not all mitochondria. The fact that we measured the sphingosine decrease in the total cells but not in the fractions isolated nevertheless suggests that not all lysosomes connect to mitochondria/MAM; specific enzymatic activities might be segregated in lysosomes depending on their localization in the cell and their interaction with other organelles. It seems that lysosomes were not massively recruited to the MF during apoptosis (Fig. 6F, supplemental Fig. S4C); the gain in ASMase activity measured in MAM may thus be linked to an activation induced by oxygen species produced in stressed mitochondria (34).

Based on our results, we can provide a subcellular timeline on ceramide and related metabolites during apoptosis. Ceramide production and especially C16-ceramide increase at the early stages of apoptosis through a possible conversion from sphingosine and SM first, then through de novo synthesis from sphinganine, all of these events happening upstream from the mitochondrial permeabilization and caspase activation (Fig. 3), while lactosyl- and glucosyl-ceramide are not affected. Sphinganine has been shown to be involved itself in apoptosis through the disruption of the mitochondrial respiratory chain and inhibition of kinase (35, 36). The regulation of contacts between organelles, including MAM, might thus be a key determinant in the regulation of sphingolipid synthesis and thereby participate to the early stage of apoptosis.⬛

REFERENCES

1. Drin, G. 2014. Topological regulation of lipid balance in cells. *Annu. Rev. Biochem.* **83:** 51–77.
2. Hannun, Y. A., and L. M. Obeid. 2008. Principles of bioactive lipid signalling: lessons from sphingolipids. *Nat. Rev. Mol. Cell Biol.* **9:** 139–150.
3. Huang, X., B. R. Withers, and R. C. Dickson. 2014. Sphingolipids and lifespan regulation. *Biochim. Biophys. Acta.* **1841:** 657–664.
4. Castro, B. M., M. Prieto, and L. C. Silva. 2014. Ceramide: a simple sphingolipid with unique biophysical properties. *Prog. Lipid Res.* **54:** 53–67.
5. Pewzner-Jung, Y., H. Park, E. L. Laviad, L. C. Silva, S. Lahiri, J. Stiban, R. Erez-Roman, B. Brugger, T. Sachsenheimer, T. Wieland, et al. 2010. A critical role for ceramide synthase 2 in liver homeostasis: I. alterations in lipid metabolic pathways. *J. Biol. Chem.* **285:** 10902–10910.
6. Stiban, J., and M. Perera. 2015. Very long chain ceramides interfere with C16-ceramide-induced channel formation: a plausible mechanism for regulating the initiation of intrinsic apoptosis. *Biochim. Biophys. Acta.* **1848:** 561–567.
7. Bonnaud, S., C. Niaudet, G. Pottier, M. H. Gaugler, J. Millour, J. Barbet, L. Sabatier, and F. Paris. 2007. Sphingosine-1-phosphate protects proliferating endothelial cells from ceramide-induced apoptosis but not from DNA damage-induced mitotic death. *Cancer Res.* **67:** 1803–1811.
8. Mignard, V., L. Lalier, F. Paris, and F. M. Vallette. 2014. Bioactive lipids and the control of Bax pro-apoptotic activity. *Cell Death Dis.* **5:** e1266.
9. Birbes, H., S. El Bawab, Y. A. Hannun, and L. M. Obeid. 2001. Selective hydrolysis of a mitochondrial pool of sphingomyelin induces apoptosis. *FASEB J.* **15:** 2669–2679.
10. Chipuk, J. E., G. P. McStay, A. Bharti, T. Kuwana, C. J. Clarke, L. J. Siskind, L. M. Obeid, and D. R. Green. 2012. Sphingolipid metabolism cooperates with BAK and BAX to promote the mitochondrial pathway of apoptosis. *Cell.* **148:** 988–1000.
11. Ardail, D., I. Popa, J. Bodennec, P. Louisot, D. Schmitt, and J. Portoukalian. 2003. The mitochondria-associated endoplasmic-reticulum subcompartment (MAM fraction) of rat liver contains highly active sphingolipid-specific glycosyltransferases. *Biochem. J.* **371:** 1013–1019.
12. Bionda, C., J. Portoukalian, D. Schmitt, C. Rodriguez-Lafrasse, and D. Ardail. 2004. Subcellular compartmentalization of ceramide metabolism: MAM (mitochondria-associated membrane) and/or mitochondria? *Biochem. J.* **382:** 527–533.
13. van Vliet, A. R., T. Verfaillie, and P. Agostinis. 2014. New functions of mitochondria associated membranes in cellular signaling. *Biochim. Biophys. Acta.* **1843:** 2253–2262.
14. Poston, C. N., S. C. Krishnan, and C. R. Bazemore-Walker. 2013. In-depth proteomic analysis of mammalian mitochondria-associated membranes (MAM). *J. Proteomics.* **79:** 219–230.
15. Paillard, M., E. Tubbs, P. A. Thiebaut, L. Gomez, J. Fauconnier, C. C. Da Silva, G. Teixeira, N. Mewton, E. Belaidi, A. Durand, et al. 2013. Depressing mitochondria-reticulum interactions protects cardiomyocytes from lethal hypoxia-reoxygenation injury. *Circulation.* **128:** 1555–1565.
16. Schon, E. A., and E. Area-Gomez. 2013. Mitochondria-associated ER membranes in Alzheimer disease. *Mol. Cell. Neurosci.* **55:** 26–36.
17. Tubbs, E., P. Theurey, G. Vial, N. Bendridi, A. Bravard, M. A. Chauvin, J. Li-Cao, F. Zoulim, B. Bartosch, M. Ovize, et al. 2014. Mitochondria-associated endoplasmic reticulum membrane (MAM) integrity is required for insulin signaling and is implicated in hepatic insulin resistance. *Diabetes.* **63:** 3279–3294.
18. Vance, J. E. 2014. MAM (mitochondria-associated membranes) in mammalian cells: lipids and beyond. *Biochim. Biophys. Acta.* **1841:** 595–609.
19. Wieckowski, M. R., C. Giorgi, M. Lebiedzinska, J. Duszynsk, and P. Pinton. 2009. Isolation of mitochondria-associated membranes and mitochondria from animal tissues and cells. *Nat. Protoc.* **4:** 1582–1590.
20. Bodennec, J., O. Koul, I. Aguado, G. Brichon, G. Zwingelstein, and J. Portoukalian. 2000. A procedure for fractionation of sphingolipid classes by solid-phase extraction on aminopropyl cartridges. *J. Lipid Res.* **41:** 1524–1531.
21. Mühle, C., H. B. Huttne, S. Walte, M. Reichel, F. Canneva, P. Lewczuk, E. Gulbins, and J. Kornhuber. 2013. Characterization of acid sphingomyelinase activity in human cerebrospinal fluid. *PLoS One.* **8:** e62912.
22. Rao, B. G., and M. W. Spence. 1976. Sphingomyelinase activity at pH 7.4 in human brain and a comparison to activity at pH 5.0. *J. Lipid Res.* **17:** 506–515.
23. Arnaudeau, S., M. Frieden, K. Nakamura, C. Castelbou, M. Michalak, and N. Demaurex. 2002. Calreticulin differentially modulates calcium uptake and release in the endoplasmic reticulum and mitochondria. *J. Biol. Chem.* **277:** 46696–46705.
24. Lewin, T. M., J. H. Kim, D. A. Granger, J. E. Vance, and R. A. Coleman. 2001. Acyl-CoA synthetase isoforms 1, 4, and 5 are present in different subcellular membranes in rat liver and can be inhibited independently. *J. Biol. Chem.* **276:** 24674–24679.
25. Gratas, C., Q. Sery, M. Rabe, L. Oliver, and F. M. Vallette. 2014. Bak and Mcl-1 are essential for Temozolomide induced cell death in human glioma. *Oncotarget.* **5:** 2428–2435.
26. Hsu, Y. T., and R. J. Youle. 1997. Nonionic detergents induce dimerization among members of the Bcl-2 family. *J. Biol. Chem.* **272:** 13829–13834.

27. Thomas, R. L., Jr., C. M. Matsko, M. T. Lotze, and A. A. Amoscato. 1999. Mass spectrometric identification of increased C16 ceramide levels during apoptosis. *J. Biol. Chem.* **274:** 30580–30588.

28. Kashkar, H., K. Wiegmann, B. Yazdanpanah, D. Haubert, and M. Kronke. 2005. Acid sphingomyelinase is indispensable for UV light-induced Bax conformational change at the mitochondrial membrane. *J. Biol. Chem.* **280:** 20804–20813.

29. Wong, Y. C., D. Ysselstein, and D. Krainc. 2018. Mitochondria-lysosome contacts regulate mitochondrial fission via RAB7 GTP hydrolysis. *Nature.* **554:** 382–386.

30. Crimi, M., and M. D. Esposti. 2011. Apoptosis-induced changes in mitochondrial lipids. *Biochim. Biophys. Acta.* **1813:** 551–557.

31. Juin, P., O. Geneste, F. Gautier, S. Depil, and M. Campone. 2013. Decoding and unlocking the BCL-2 dependency of cancer cells. *Nat. Rev. Cancer.* **13:** 455–465.

32. Hayashi, T., R. Rizzuto, G. Hajnoczky, and T. P. Su. 2009. MAM: more than just a housekeeper. *Trends Cell Biol.* **19:** 81–88.

33. Hernandez-Corbacho, M. J., M. F. Salama, D. Canals, C. E. Senkal, and L. M. Obeid. 2017. Sphingolipids in mitochondria. *Biochim. Biophys. Acta.* **1862:** 56–68.

34. Kornhuber, J., C. Rhein, C. P. Muller, and C. Muhle. 2015. Secretory sphingomyelinase in health and disease. *Biol. Chem.* **396:** 707–736.

35. Nagahara, Y., T. Shinomiya, S. Kuroda, N. Kaneko, R. Nishio, and M. Ikekita. 2005. Phytosphingosine induced mitochondria-involved apoptosis. *Cancer Sci.* **96:** 83–92.

36. Zigdon, H., A. Kogot-Levin, J. W. Park, R. Goldschmidt, S. Kelly, A. H. Jr Merrill, A. Scherz, Y. Pewzner-Jung, A. Saada, and A. H. Futerman. 2013. Ablation of ceramide synthase 2 causes chronic oxidative stress due to disruption of the mitochondrial respiratory chain. *J. Biol. Chem.* **288:** 4947–4956.